CONF-8410142--38

AGING OF CAST DUPLEX STAINLESS STEELS IN LWR SYSTEMS*

O. K. Chopra and H. M. Chung

Materials Science and Technology Division
Argonne National Laboratory
Argonne, Illinois 60439

CONF-8410142--38

DE85 003023

October 1984

MASTER

DISCLAIMER

To be presented at the 12th Water Reactor Safety Research Information Meeting, October 22-26, 1984, National Bureau of Standards (NBS), Gaithersburg, MD.

*Work supported by the Office of Nuclear Regulatory Research, U. S. Nuclear Regulatory Commission.

AGING OF CAST DUPLEX STAINLESS STEELS IN LWR SYSTEMS*

O. K. Chopra and H. M. Chung

Materials Science and Technology Division
Argonne National Laboratory
Argonne, Illinois 60439

Abstract

A program is being conducted to investigate the significance of in-service embrittlement of cast duplex stainless steels under light-water reactor operating conditions. The existing data are evaluated to determine the expected embrittlement of cast components during the operating lifetime of reactors and to define the objectives and scope of the investigation. This presentation describes the status of the program. Data for the metallurgical characterization of the various cast stainless steels used in the investigation are presented. Charpy impact tests on short-term aged material indicate that CF-3 stainless steels are less susceptible to embrittlement than CF-8 or CF-8M stainless steels. Microstructural characterization of cast stainless steels that were obtained from Georg Fischer Co. and aged for up to 70,000 h at 300, 350, and 400°C reveals the formation of four different types of precipitates that are not α'. Embrittlement of the ferrite phase is primarily due to pinning of the dislocations by two of these precipitates, designated as Type M and Type X. The ferrite phase is embrittled after ~8 yr at 300°C and shows cleavage fracture. Examination of the fracture surfaces of the impact-test specimens indicates that the toughness of the long-term aged material is determined by the austenite phase.

Introduction

Cast duplex stainless steels are used extensively in the nuclear industry. The ferritic phase in the duplex structure of austenitic-ferritic stainless steels increases the tensile strength and improves weldability, resistance to stress corrosion, and soundness of casting of these steels. However, various carbide phases, intermetallic compounds such as sigma and chi phase, and the chromium-rich BCC phase (α') can precipitate in the ferrite phase during service at elevated temperatures and lead to substantial variations in mechanical properties. It is well known that formation of sigma phase greatly reduces the toughness of cast duplex stainless steels.[1] Long-term aging at relatively low temperatures, i.e., 300 to 500°C, causes drastic reductions in the impact strength of these steels.[2-5] Data on the aging behavior of ferritic or austenitic-ferritic steels show no evidence of sigma-phase formation at temperatures below 550°C. The mottled appearance characteristic of α' precipitates has been observed in material aged at temperatures between 450 and 500°C.[6-8] Microstructural studies on cast duplex stainless steel that were aged for up to 70,000 h at 400, 350, and 300°C revealed the formation of three different types of precipitates which are not α'.[8] At the

*Work supported by the Office of Nuclear Regulatory Research, U. S. Nuclear Regulatory Commission.

operating temperatures of light-water reactors (LWRs), i.e., 280 to 320°C, embrittlement of cast stainless steels is probably caused by the formation of these as yet unidentified precipitates in the ferrite phase.

In general, thermal aging of cast duplex stainless steels at temperatures between 300 and 450°C causes an increase in hardness and tensile strength and a decrease in ductility, Charpy impact strength, and J_{IC} fracture toughness of the material. The low-cycle fatigue properties and fatigue crack propagation are not significantly modified by aging.[4,5] The room-temperature impact strength can be reduced by ~80% after aging for ~70,000 h at temperatures as low as 300°C.[2] The ferrite content of the cast structure has a pronounced influence on the embrittlement behavior, namely, an increase in ferrite content increases the susceptibility to embrittlement.

Extensive data on embrittlement of single-phase binary Fe-Cr ferritic alloys indicate significant effects of chemical composition on the aging behavior. An increase in chromium, molybdenum, or titanium content in the ferrite phase enhances the rate as well as the extent of embrittlement.[6] Interstitial elements, such as carbon and nitrogen, also accelerate embrittlement of single-phase ferritic steels.[9,10] Unfortunately, the bulk of this work has been carried out at temperatures >400°C, and extrapolation of the results to reactor temperatures may not be valid. Furthermore, the influence of metallurgical variables such as grain structure and ferrite morphology has not been established.

The kinetics of embrittlement are evaluated by considering the aging phenomenon to be a thermally activated process described by an Arrhenius relation. The activation energy is determined by examining the degree of embrittlement produced by different time-temperature histories. Arrhenius extrapolations can be used to determine the equivalent aging time at different temperatures:

$$t = 10^{P} \exp\left[\frac{Q}{R}\left(\frac{1}{T} - \frac{1}{673}\right)\right], \qquad (1)$$

where Q is the activation energy, R the gas constant, T the absolute temperature, and P an aging parameter which represents the degree of aging reached after 10^{P} h at 400°C. The activation energy for the process of embrittlement has been described as a function of chemical composition of the cast material.[5] Thus,

$$Q\ (\text{kJ/mole}) = -182.6 + 19.9\ (\%\ \text{Si}) + 11.08\ (\%\ \text{Cr}) + 14.4\ (\%\ \text{Mo}). \qquad (2)$$

Chemical compositions of the various cast materials included in low-temperature aging studies yield activation energies between 65 and 100 kJ/mole (~15 and 24 kcal/mole) for cast CF-8 or CF-3 stainless steels and between 75 and 105 kJ/mole (~18 and 25 kcal/mole) for cast CF-8M stainless steel. The room-temperature impact energies of cast stainless steels that were aged for up to 70,000 h at 300, 350, and 400°C (Ref. 2) are plotted as a function of the parameter P in Figs. 1 and 2. The activation energies for the different materials were calculated from Eq. (2).

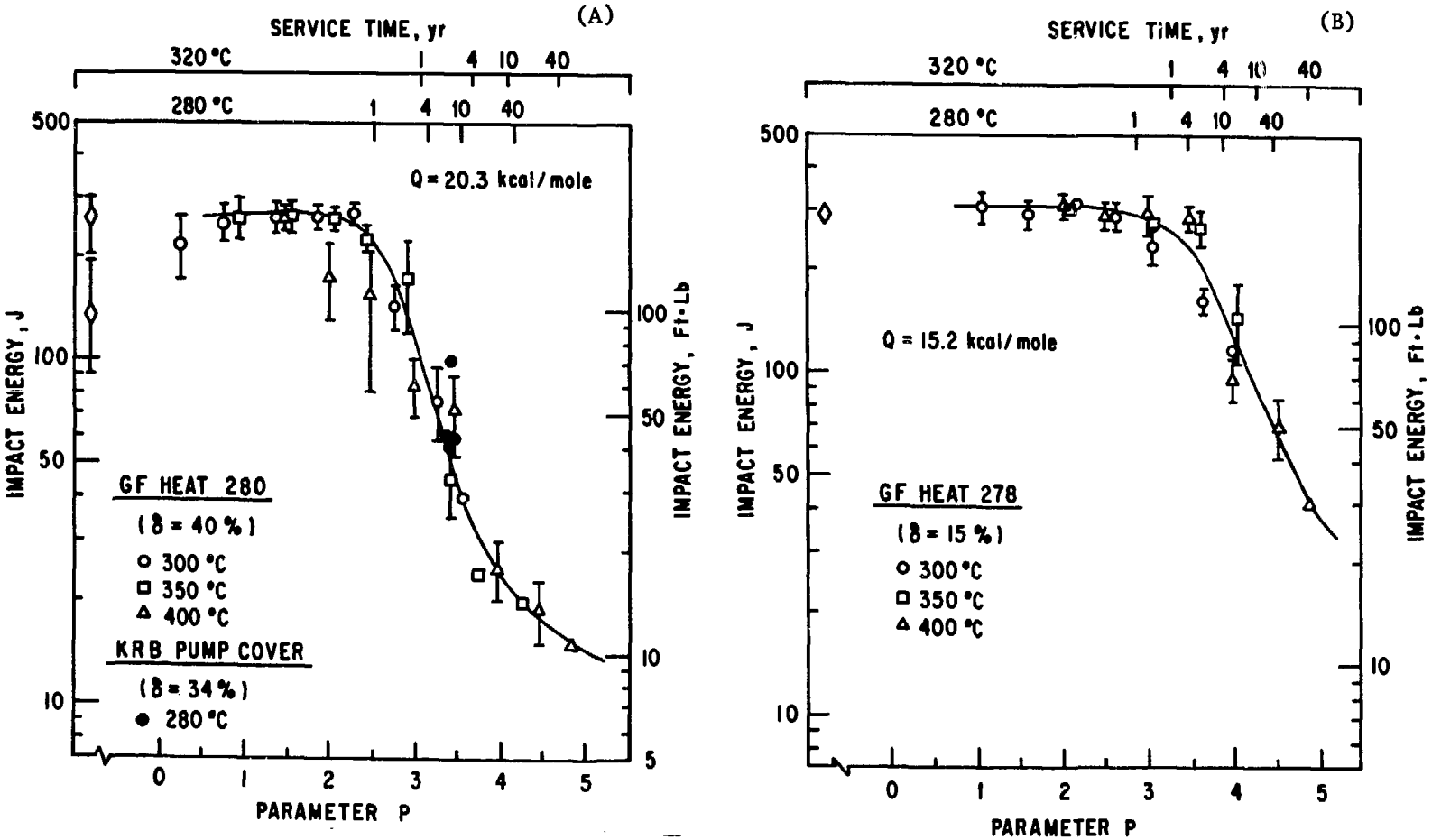

Fig. 1. Effect of Thermal Aging on the Impact Energy of Cast CF-8 Stainless Steels Containing (A) >30% Ferrite and (B) 15% Ferrite.

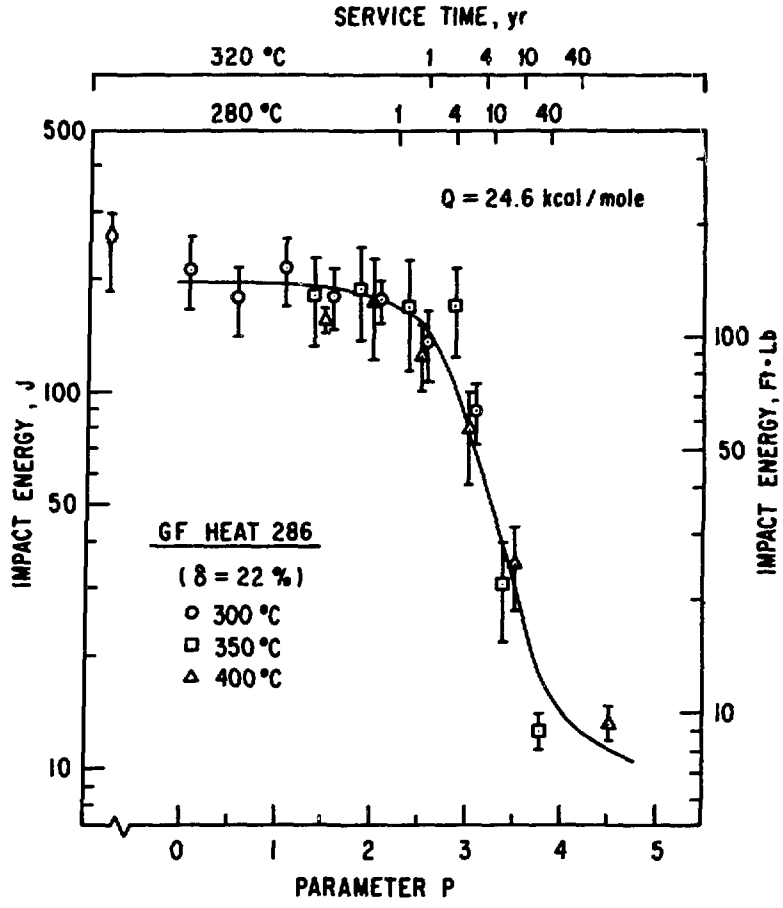

Fig. 2. Effect of Thermal Aging on the Impact Energy of Cast CF-8M Stainless Steel Containing 22% Ferrite.

For each material, the results for an aging temperature of 300°C follow the data for higher aging temperatures. However, the time and temperature for the onset of embrittlement is different for different materials. Cast stainless steels containing >20% ferrite [Figs. 1(A) and 2] show drastic reduction in impact strength for P values >2. Cast CF-8 material containing ~15% ferrite [Fig. 1(B)] shows a reduction in impact strength only above a P value of 3 and the degree of embrittlement is significantly less than for the material containing 40% ferrite. Experimental data obtained on CF-8 steel from the pump cover of the KRB reactor[11] are also plotted in Fig. 1(A). The material was in service for ~8 yr at 280°C. The results show good agreement with data obtained on laboratory-aged material. Figures 1 and 2 may be used to predict the impact energy of cast stainless steels after long-term service at reactor operating temperatures. For example, the impact energy of cast CF-8 steel (containing 30-40% ferrite) or CF-8M steel (containing 20-25% ferrite) will decrease below 70 J (50 ft•lb) after ~2 yr service at 320°C or ~7 yr service at 280°C.

Figure 3 shows the predicted impact strength for various service conditions of CF-8 material (containing 30-40% ferrite), aged at 280 and 320°C during long-term service. The ductile-brittle transition temperature (DBTT) curve was calculated from a tanh function given by

$$K = K_o + B\left[1 + \tanh\left\{\frac{(T - T_o)m + B - B_o}{B}\right\}\right], \qquad (3)$$

where K_o is the lower shelf value of the transition curve and B_o is half the difference between the upper and lower shelf. The coefficients T_o, B, and m depend on aging. Initial values of the constants were determined from DBTT data for the unaged material from the KRB pump cover. The change in coefficients T_o, B, and m with thermal aging is assumed to be the same as that for Heat 280N investigated by Georg Fischer Co. (Ref. 2). The predicted curve for 70,000 h of service at 280°C shows fair agreement with the experimental results, as shown in Fig. 3 (upper panel). The DBTT curve for service at 320°C indicates large reductions in upper shelf values after 70,000 h (~8 yr) of service, and impact energies below 70 J at temperatures up to 120°C. However, the room-temperature impact energy after 300,000 h of service is higher than that indicated by Fig. 1(A). For example, Fig. 3 predicts a room-temperature impact energy of ~40 J after 300,000 h (~34 yr) of service at 320°C, whereas a value of ~20 J is predicted from data shown in Fig. 1(A). The DBTT curves shown in Fig. 3 are current "best estimates" and are subject to large uncertainties. DBTT data for low-temperature aged material are required to accurately establish the change in transition curve due to thermal aging.

To demonstrate the validity of using such an Arrhenius extrapolation of high-temperature data to predict the long-term embrittlement of cast stainless steels at reactor operating temperatures requires a satisfactory understanding of the aging process. The mechanism of embrittlement needs to be established to ensure that the activation energy obtained from the laboratory tests is representative of the actual process. The activation energies determined from the aging data are much lower than that expected for a mechanism controlled by solute bulk diffusion (i.e., activation energy of 230 kJ/mole). This indicates that processes other than precipitation of additional phases in the ferrite matrix contribute to embrittlement of cast duplex stainless steels. For example, microstructural modifications of the austenite phase or changes in the fracture behavior of duplex material may influence the notch toughness of cast stainless steels. The available information is not sufficient to correlate the microstructure with the mechanical properties or to determine the mechanism of low-temperature embrittlement.

The objectives of this program are to (1) characterize the microstructure of in-service reactor components and laboratory-aged material, correlate it with loss of fracture toughness, and identify the mechanism of embrittlement; (2) determine the validity of laboratory-induced embrittlement data for predicting the toughness of component materials after long-term aging at reactor operating temperatures; (3) characterize the loss of fracture toughness in terms of fracture mechanics parameters in order to provide the data needed to assess the safety significance of embrittlement; and (4) provide additional understanding of the effects of key compositional and metallurgical variables on the kinetics and degree of embrittlement.

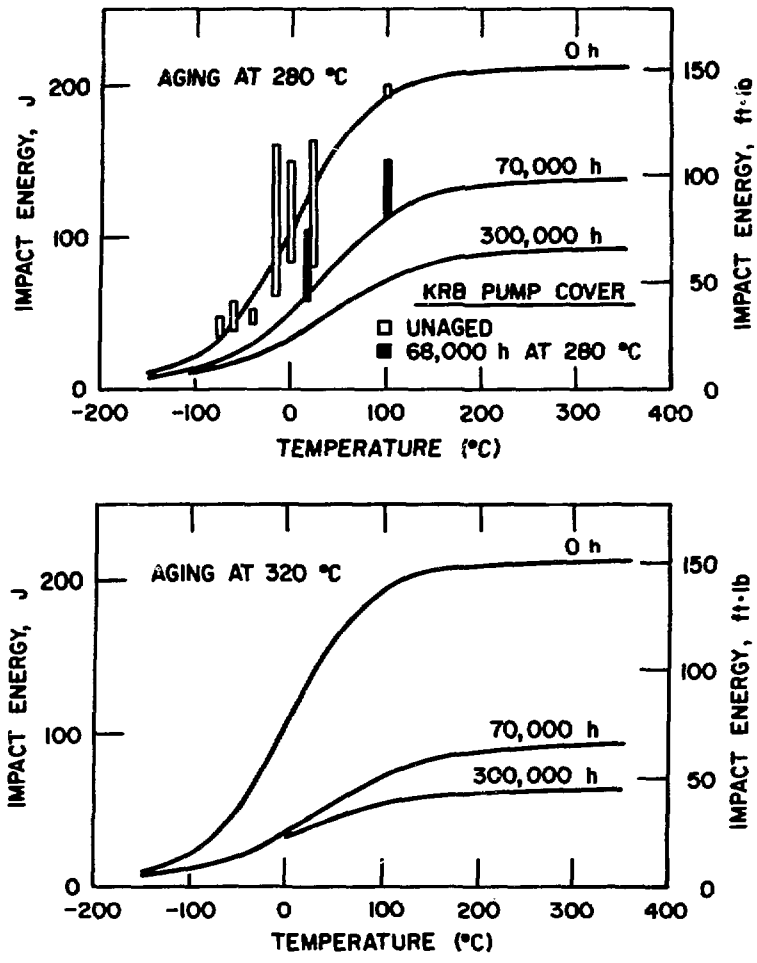

Fig. 3. Effect of Thermal Aging at 280 and 320°C on the Transition Curves for Impact Energy of Cast CF-8 Stainless Steel.

The relationship between aging time and temperature for onset of embrittlement will be determined by microstructural examination and measurements of hardness, Charpy impact strength, tensile strength, and J_{IC} fracture toughness. The kinetics and fracture toughness data generated in this program and from other sources will provide the technical basis to define the aging histories, chemical compositions, and metallurgical structures that lead to significant embrittlement of cast stainless steels under LWR operating conditions. Estimates of the degree of embrittlement will be compared with data obtained from examination of material from actual reactor service. Data pertaining to the effects of compositional and metallurgical variables on the embrittlement phenomenon will help to evaluate the possible remedies for existing and future plants.

Material Procurement and Characterization

Material was obtained from various experimental and commercial heats of CF-8, -8M, and -3 grades of cast stainless steel. Nineteen experimental heats

were obtained in the form of keel blocks approximately 180 mm long and 120 mm high, with a thickness that tapered from 30 to 90 mm. The compositions of the heats were varied to provide different concentrations of nickel, chromium, carbon, and nitrogen in the material and ferrite contents in the range of 3 to 30%. Six large experimental heats, in the form of 76-mm-thick slabs, were obtained for J_R-curve testing. Sections from four centrifugally cast pipes (grades CF-3, -8, and -8M), a static-cast pump impeller (grade CF-3), and a static-cast pump casing ring (grade CF-8) were also procured. The outer diameter and wall thickness of the cast pipes range from 0.6 to 0.9 m and 38.1 to 76.2 mm, respectively.

A cover plate assembly of cast stainless steel from the recirculating pump of the KRB reactor (the same one shown in Fig. 1) was also procured. The material was in service for ~12 yr at 280°C. The cover plate is 0.89 m in diameter and 0.32 m deep. The thicknesses of the various sections range from 60 to 120 mm. The ferrite content of the cast material is ~34%. The cover plate assembly was decontaminated and samples are being obtained from different sections of the plate for mechanical testing and microstructural characterization.

Charpy impact specimen blanks were prepared from keel blocks of the experimental heats and material from the various reactor components. Blanks for compact tension specimens were obtained from sections of two centrifugally cast pipes, the static-cast pump casing ring, the static-cast pump impeller, and the cast slabs. The specimen blanks are being aged at 450, 400, 350, 320, and 290°C for times up to 50,000 h. The test matrices for the various mechanical tests and microstructural examination have been presented earlier.[12] The mechanical test specimens were machined after the thermal aging treatment. The orientations of the notches for the Charpy impact and compact tension specimens were both L-C and C-L.*

The various cast materials were examined to characterize the chemical composition, hardness, ferrite content, ferrite morphology, and grain structure. Energy dispersive x-ray analyses (EDAX) were performed to determine the composition of the α and γ phases (i.e., ferrite and austenite phases) of the duplex structure. All castings were examined in the three orientations, i.e., longitudinal, circumferential, and radial planes, as well as different locations, namely, material near the center and the inner and outer surfaces of the pipes, and top (Row 6) and bottom (Row 3) regions of the keel blocks. Orientation of the material had little or no effect on either hardness or ferrite content and morphology. The ferrite morphology in the various cast materials was globular for ferrite contents of <5%, lacy for ferrite contents between 5 and 20%, and acicular for material with larger amounts of ferrite. The ferrite morphology in the keel blocks was different from that in the centrifugally cast pipes. For the same ferrite content, the islands of ferrite in the keel blocks were smaller and had a finer dispersion than in the pipe material.

The chemical composition, hardness, and ferrite content of the various heats of cast stainless steel are given in Table 1. The results show some

*L = longitudinal or axial and C = circumferential or transverse. The first letter designates the direction normal to the crack plane and the second letter the expected direction of crack propagation.

TABLE 1. Chemical Composition, Hardness, and Ferritic Content of the Various Heats of Cast Stainless Steel

Heat	Grade	Composition,[a] wt %							Location	Hardness, R_B	Ferrite Content,[b] %
		Mn	Si	Mo	Cr	Ni	N	C			
					Cast Keel Blocks						
58	CF-8	0.66	1.21	0.29	19.56	10.37	0.040	0.050	Row 3	76.0	3.6
									Row 6	78.2	2.1
57		0.69	1.24	0.28	18.45	8.94	0.041	0.060	Row 3	80.1	5.1
									Row 6	80.3	2.8
54		0.58	1.08	0.31	19.42	8.91	0.073	0.065	Row 3	82.6	1.2
									Row 6	83.9	2.3
53		0.70	1.28	0.35	19.62	8.86	0.045	0.070	Row 3	82.6	9.5
									Row 6	83.6	7.8
56[c]		0.60	1.16	0.30	19.33	8.93	0.031	0.060	Row 3	81.9	11.9
									Row 6	83.1	8.2
59		0.63	1.14	0.26	20.35	8.95	0.040	0.070	Row 3	83.5	14.2
									Row 6	82.8	12.7
61		0.70	1.20	0.27	20.54	8.59	0.060	0.060	Row 3	85.1	13.0
									Row 6	85.5	13.1
60[c]		0.71	1.01	0.26	21.02	8.07	0.050	0.070	Row 3	86.2	20.4
									Row 6	87.2	21.7
50	CF-3	0.67	1.26	0.28	17.63	8.84	0.064	0.019	Row 3	79.6	5.0
									Row 6	80.6	3.7
49		0.66	1.11	0.29	19.32	10.10	0.064	0.022	Row 3	76.1	8.0
									Row 6	77.2	6.3
48		0.67	1.21	0.26	19.42	9.90	0.071	0.016	Row 3	77.6	8.9
									Row 6	78.6	8.5
47		0.65	1.23	0.45	19.67	10.04	0.027	0.018	Row 3	79.0	16.5
									Row 6	80.3	16.2
52		0.63	1.04	0.31	19.51	9.07	0.049	0.021	Row 3	81.4	10.3
									Row 6	81.8	16.7
51[c]		0.66	1.06	0.28	20.36	8.69	0.048	0.023	Row 3	83.7	18.0
									Row 6	83.9	18.0
62	CF-8M	0.84	0.64	2.46	18.38	11.35	0.030	0.070	Row 3	78.2	6.3
									Row 6	78.0	2.6
63		0.69	0.75	2.52	19.39	11.22	0.030	0.050	Row 3	81.0	10.9
									Row 6	82.1	10.0

TABLE 1. (Contd.)

Heat	Grade	Composition,[a] wt % Mn	Si	Mo	Cr	Ni	N	C	Location	Hardness, R_B	Ferrite Content,[b] %
66[c]	CF-8M	0.71	0.60	2.36	19.41	9.13	0.030	0.060	Row 3	84.6	19.2
									Row 6	85.8	20.5
65		0.66	0.63	2.53	20.95	9.39	0.060	0.060	Row 3	88.4	21.4
									Row 6	89.5	25.4
64[c]		0.70	0.71	2.41	20.87	9.01	0.030	0.050	Row 3	89.7	27.5
									Row 6	89.7	29.3
						Cast Components					
C1	CF-8	1.22	1.19	0.64	19.10	9.32	0.041	0.036	O.D.	78.3	2.3
					18.89	9.42			I.D.	80.6	1.7
P1		0.56	1.07	0.04	20.38	8.00	0.053	0.032	O.D.	84.5	27.6
					20.60	8.20			I.D.	85.3	19.5
P3	CF-3	1.04	0.86	0.01	18.93	8.33	0.159	0.020	O.D.	80.6	2.5
					18.85	8.56			I.D.	83.7	0.9
P2		0.72	0.92	0.16	20.20	9.24	0.041	0.020	O.D.	82.4	15.9
					20.20	9.51			I.D.	85.1	13.2
I		0.46	0.80	0.44	20.08	8.50	0.030	0.016	Vane 3	81.1	20.2
					20.20	0.80			Vane 1	82.2	14.3
					20.34	8.64			Shroud	78.1	16.9
					20.20	8.84			Hub	81.0	19.1
P4	CF-8M	1.07	1.02	2.06	19.63	10.00	0.153	0.039	O.D.	83.0	11.1
					19.65	9.99			I.D.	83.2	9.8

[a]Chemical composition of the keel blocks supplied by the vendor.
[b]Ferrite content measured by Ferrite Scope, Auto Test FE, Probe Type FSP-1.
[c]Chemical composition of the large experimental heats.

differences in hardness and ferrite content for material from different locations in the castings. The ferrite content is lower and the hardness is slightly higher toward the inner surface of the various cast pipes. This behavior appears to be related to the nickel content in the material, i.e., the concentration of nickel is higher near the inner surface. Differences in hardness and ferrite content are also observed for material from different locations in the static-cast keel blocks. Hardness is always higher toward the top of the keel blocks. However, variations in the ferrite content depend on the Cr_{eq}/Ni_{eq} ratio in the material; the ferrite content toward the top of the casting is lower for material with Cr_{eq}/Ni_{eq} <1.13 and higher for material with Cr_{eq}/Ni_{eq} >1.13. In general, the hardness of the cast material increases with an increase in ferrite content. For the same ferrite content, the hardness of CF-8 and -8M material is comparable while the hardness of CF-3 material is lower. An increase in nitrogen content increases the hardness of all grades of cast stainless steel.

The ferrite content and the different structures present in the four pipe sections and pump casing ring are listed in Table 2. The grain structures were examined in the axial, circumferential, and radial planes. Two castings, P1 and P2, contained equiaxed grains across the entire thickness of the pipe.

TABLE 2. Ferrite Content and Grain Structure of Various Cast Stainless Steel Pipes

Heat	OD, m	Wall, mm	Process	Grade	Ferrite Content,[a] % OD	Ferrite Content,[a] % ID	Grain Structure
C1	0.60	57.1	Static	CF-8	2.3	1.7	Banded, columnar/equiaxed; radial to axial growth near ends
P1	0.89	63.5	Centr.	CF-8	27.6	19.5	Equiaxed across thickness
P3	0.58	51.6	Centr.	CF-3	2.5	0.9	Banded, radially oriented columnar; one equiaxed band (~4 mm deep) near ID
P2	0.93	73.0	Centr.	CF-3	15.9	13.2	Equiaxed across thickness
P4	0.58	31.8	Centr.	CF-8M	11.1	9.8	Radially oriented columnar

[a]Ferrite content measured by Ferrite Scope, Auto Test FE, Probe Type FSP-1.

The grain size and distribution were not significantly different in the three orientations. The equiaxed grains were probably produced intentionally by a low pouring temperature or by shear between the liquid and solid. The shear could cause dendrite arms to break off and disperse in the liquid-solid region. These castings are expected to exhibit uniform properties in all directions. The other two centrifugally cast pipes, P3 and P4, showed radially oriented columnar grains. Pipe section P3 also contained a band of small equiaxed grains near the inner surface. This band was relatively thin, i.e., ~4 mm deep, and probably formed accidentally. The columnar grain castings are expected to have uniform properties in the axial and circumferential directions. The static-cast pump casing ring, keel blocks, and slab showed a mixed structure of columnar and equiaxed grains.

EDAX analyses of the various cast materials indicate that the concentration of Cr, Mo, and Si is higher in the α phase and Ni is higher in the γ phase. The concentration of Mn, C, and N is expected to be higher in the γ phase. The results indicate that an increase in the ferrite content of the duplex material has little or no effect on the concentration of Ni in the two phases. For the various cast materials, the average Ni content in the α and γ phases was 4.8 ± 0.4 and 8.7 ± 0.4 wt %, respectively. The concentration of Cr in both phases increases slightly with an increase in the ferrite content. The Cr content in the α phase increases from ~25 wt % for a cast material with 2% ferrite to ~26.1 wt % for a casting with 30% ferrite. The corresponding values of the Cr content in the γ phase are ~19.2 and 20.4 wt %, respectively. These results indicate that the precipitation reactions in the α phase should not be significantly different for cast stainless steels containing different amounts of ferrite. The strong effect of ferrite content on the impact energy

of cast material is most likely due to the different distribution and morphology of the ferrite phase. Precipitate reactions involving the interstitial elements may also influence the mechanical properties of the aged material.

Mechanical Properties of Aged Material

Charpy-impact tests were conducted at room temperature on material that was aged for up to 3000 h at 450, 400, and 350°C. As expected, thermal aging of the cast stainless steels decreased the impact energy. The data indicate that the reduction in impact strength depends not only on the ferrite content, but also on the grain structure and grade of the material. Thermal aging of cast stainless steels with >10% ferrite resulted in substantial reduction in impact energy, whereas cast materials with <10% ferrite showed little or no decrease in impact energy. The CF-3 grades of cast materials exhibit greater resistance to embrittlement relative to the CF-8 and CF-8M grades. For example, the impact energy for Heats 47 and 52 of CF-3 steels decreased by ~25% after aging for 3000 h at 450°C, while Heats 59 and 61 of CF-8 steels showed ~50% reduction in impact energy after a similar aging treatment. Data also indicate superior notch toughness for the centrifugally cast pipe material (e.g., Heat P2) relative to the static-cast keel blocks. Charpy-impact tests are in progress on material that was aged at lower temperatures and material from the pump cover of the KRB reactor.

Microstructural Characterization of the Aged and Impact-tested Material

Results of microstructural characterization by transmission electron microscopy (TEM) of several ferritic alloys and cast duplex stainless steels (aged at 300-475°C) have been reported previously.[8] A total of five different types of precipitates have been identified in the ferrite phase. These can be summarized as follows:

(1) α' - chromium-rich phase giving rise to mottled bright-field images but producing no detectable changes in the diffraction patterns;

(2) Type P - platelet precipitate producing strong strain-field contrast in bright-field images and giving rise to streaking of the ferrite diffraction spots;

(3) Type M - $M_{23}C_6$-like precipitate rich in Ni and Si and exhibiting a distinct diffraction pattern that contains superlattice spots with a lattice constant slightly larger than the $M_{23}C_6$ phase;

(4) Type X - precipitates observed on dislocations giving rise to very weak and streaked reflections as a result of small volume fraction and very fine size;

(5) Type ML - precipitates observed in association with Type M, coating the Type M precipitates and dislocations.

The various materials and aging conditions for which the different precipitates were observed are summarized in Table 3. The α' phase was observed in all alloys aged at 475°C, i.e., 26Cr-1Mo and 29Cr-4Mo-2Ni ferritic steels

TABLE 3. Summary of Types of Precipitates Observed in Ferritic Alloys and Cast Duplex Stainless Steel after Long-term Aging at 300-475°C

Alloy	Aging Conditions		Precipitate Phases				
	Temp., °C	Time, h	α'	Type P	Type M	Type X	Type ML
26Cr-1Mo ferritic	475	1,000	Yes				
	400	1,000	No	No			
29Cr-4Mo-2Ni ferritic	475	1,000	Yes	Yes			
	400	1,000	No	Yes			
Cast duplex stainless steel CF-8, Heat B	475	1,000	Yes		Yes		
	400	1,000	No	No	No	No	No
Cast duplex stainless steel CF-8, Heat 280	400	66,650	No		Yes	Yes	
	400	10,000	No		Yes	Yes	
	300	70,000	No		Yes	Yes	
Cast duplex stainless steel CF-8, Heat 278	400	70,000	No		Yes		
	350	70,000	No		Yes	Yes	
	300	70,000	No		Yes	Yes	
Cast duplex stainless steel CF-8M, Heat 286	400	10,000	No		Yes		Yes

and cast duplex stainless steel CF-8, Heat B. However, two heats of cast duplex stainless steel that were obtained from Georg Fischer Co. and aged up to 8 yr at 300 to 400°C did not show the α' phase. Since long-term aging at the lower temperatures is more prototypic of reactor operating conditions, TEM characterization was focused on the materials obtained from Georg Fischer Co. Characterization by scanning electron microscopy (SEM) was also conducted on the fracture surfaces of the specimens, which were impact-tested at room temperature.

1. TEM Characterization of Precipitates in Aged Cast Duplex Stainless Steel

Examination of the cast duplex stainless steel CF-8 material (Heat 280, ferrite content ~40%), aged at 400°C for 66,650 h, showed another type of precipitate in addition to those indicated in Table 3; this precipitate was designated tentatively as Type S.[13] The presence of the Type S phase could be detected only through a very careful examination of the diffraction patterns. The Type S reflections were extremely weak, indicating a small volume fraction, and could barely be detected on the microscope screen. As a result, no dark-field images could be obtained. The weak spots could be detected only from the developed negatives of the SAD pattern. The specks are very sharp compared to reflections from the matrix or Type M phases,

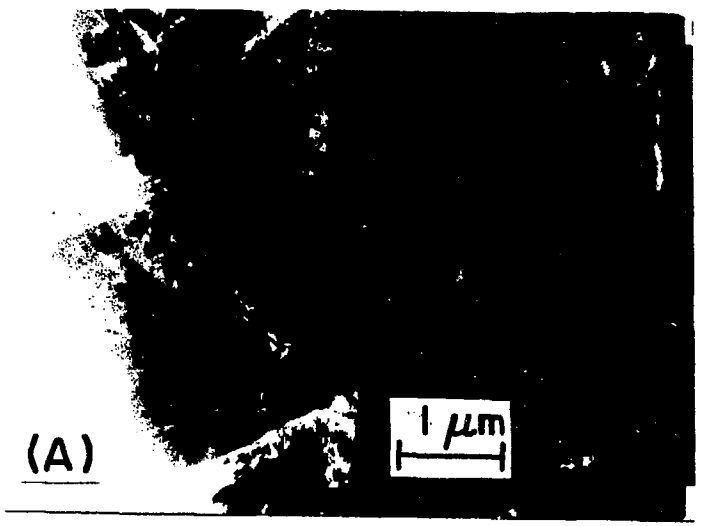

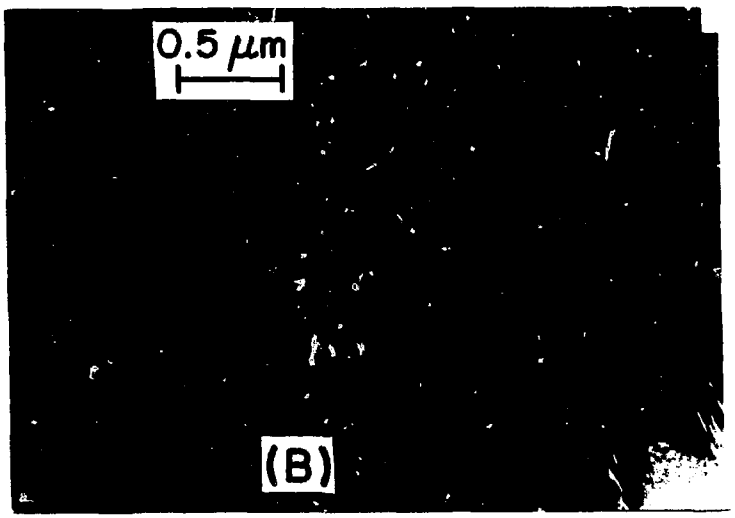

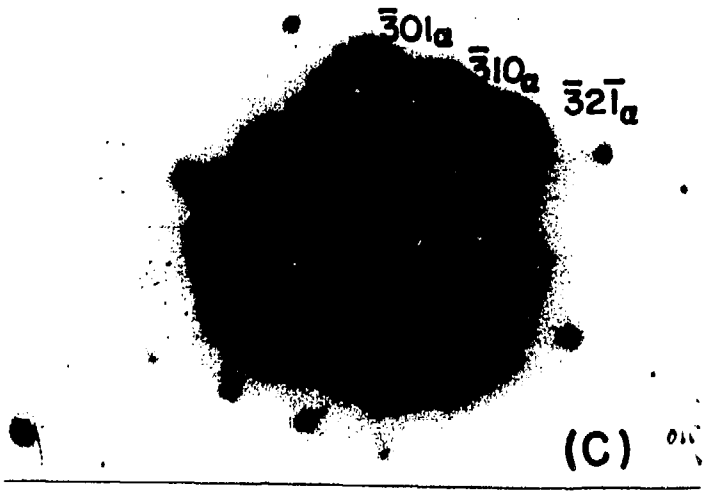

Fig. 4.

TEM Micrographs of Cast CF-8 Stainless Steel (Heat 280) after Aging at 300°C for 70,000 h (8 yr). (A) Bright-field image showing austenite (left) and ferrite (right) grains; (B) higher magnifications of the ferrite grain showing Type M ($M_{23}C_6$-like) precipitates near dislocations; (C) selected-area diffraction pattern of (B). No precipitate reflections are visible in (C) because of the low density.

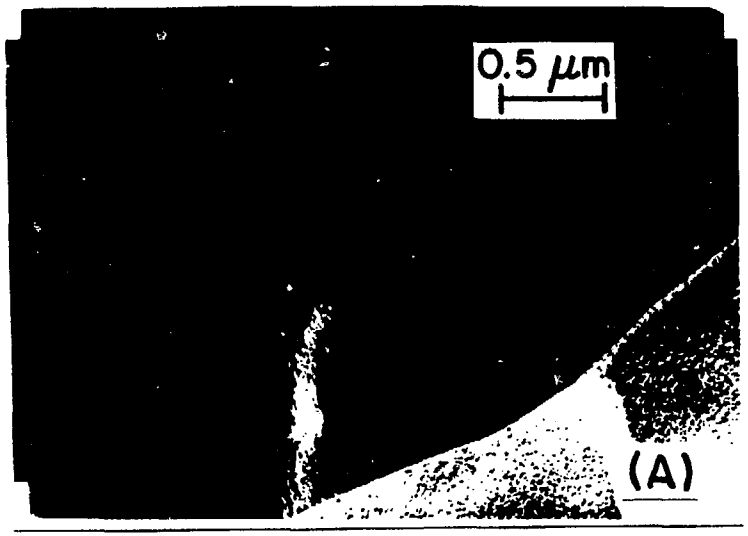

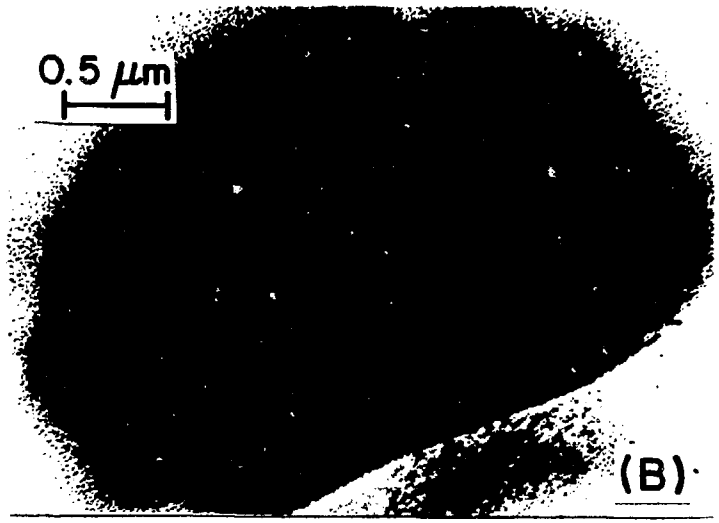

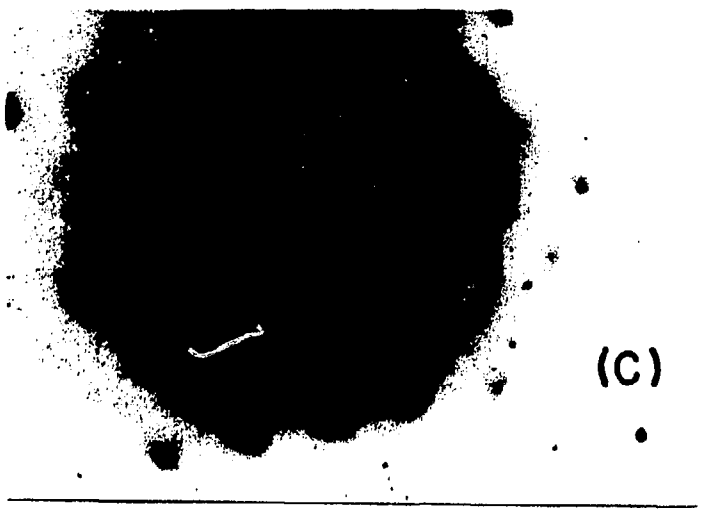

Fig. 5.

TEM Micrographs Similar to Fig. 4 but after Aging at 400°C for 66,650 h (7.6 yr). (A) Bright-field image; (B) dark-field image; (C) selected-area diffraction pattern. Note the high density of Type M precipitates and the negligible number of dislocations.

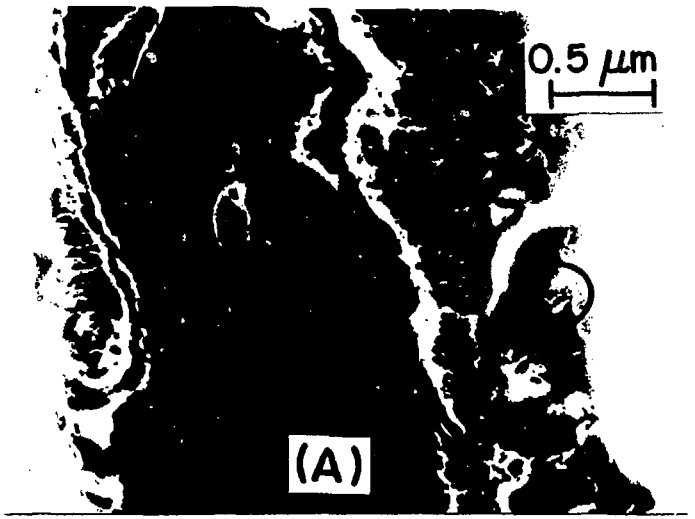

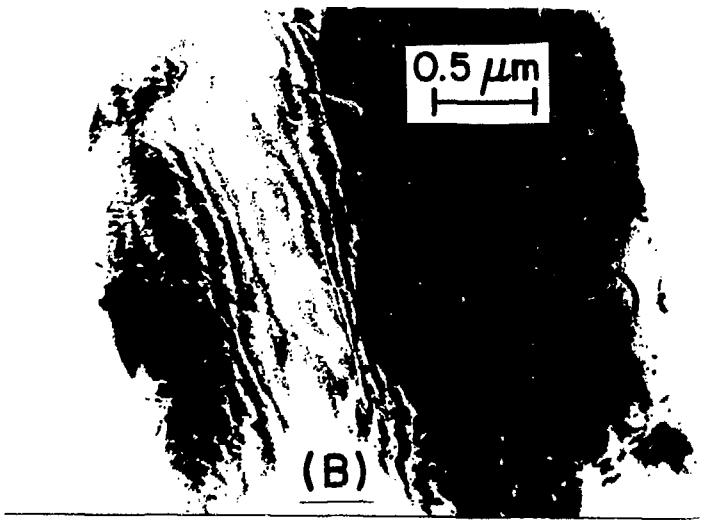

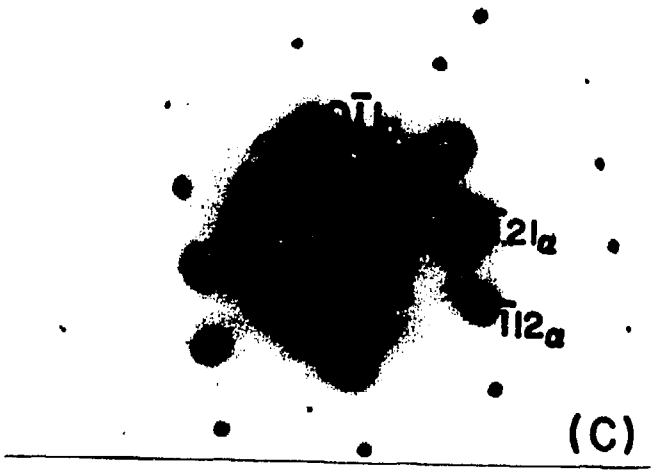

Fig. 6.

TEM Micrographs of Cast CF-8 Stainless Steel (Heat 278) after Aging at 300°C for 70,000 h (8 yr). (A) Bright-field and (B) dark-field images showing short dislocations decorated by Type X precipitates; (C) selected-area diffraction pattern showing diffuse weak Type X precipitate reflections in the circles.

indicating that the reflecting sphere intersects thin, flattened, needle-like reciprocal lattice rods. The Type S precipitates were also observed for specimens of cast duplex stainless steel CF-8, Heat 278 (ferrite content 15%) aged at 300°C for 70,000 h.

TEM examination of material aged for long times at low temperatures indicates that Type M and X precipitates, rather than the α' phase, influence the toughness and fracture behavior of cast duplex stainless steels aged at temperatures of <400°C. Both Type M and X precipitates are present in the ferrite phase of the duplex structure. However, the relative densities of the two types of precipitates are not uniform for the different specimens and ferrite grains. These precipitates are observed primarily near dislocations, indicating some degree of immobilization of the dislocations by the precipitates. Figure 4(B) shows an example of bright-field images of dislocations on the ferrite phase of Heat 280 aged at 300°C for ~8 yr (parameter P = 3.99). A relatively small number of Type M precipitates, ~10 nm in size, can be observed near the dislocations. Because of the low density of the precipitates, no extra reflections are detected in the corresponding selected-area diffraction (SAD) pattern, Fig. 4(C). In contrast, the same material (i.e., Heat 280) aged at 400°C for 7.6 yr (parameter P = 4.83) shows a negligible number of dislocations [Fig. 5(A)], a large density of Type M precipitates [Figs. 5(A) and (B)], and distinct precipitate reflections in the SAD pattern [Fig. 5(C)].

Figure 6 shows an example of dislocations in the ferrite phase, immobilized by Type X precipitates. The bright- and dark-field images of Figs. 6(A) and (B), obtained from a thin-foil specimen of Heat 280 aged at 300°C for 8 yr (parameter P = 3.70), show numerous short dislocations decorated by the Type X precipitates. The diffuse weak reflections of the Type X precipitates are denoted by small circles in the corresponding SAD pattern of Fig. 6(C).

The results from TEM examination of the microstructures of the cast duplex stainless steel materials subjected to long-term aging (e.g., at 300°C for 8 yr) indicate that dislocation glide in the ferrite phase would be significantly limited because of the preferential precipitation of Type M and X particles on or around the dislocations. In contrast, the structure of the austenite phase is characterized by a high density of dislocations and numerous stacking faults and is relatively free of precipitates, as shown in Fig. 4(A). This indicates that the overall ductility of the long-term aged duplex steel will be primarily sustained by the austenite phase. TEM characterization of the material from the pump cover of the KRB reactor is in progress.

2. SEM Fractographic Characteristics

Fracture characteristics of the impact test specimens of cast duplex stainless steel obtained from the Georg Fischer Co. were examined by SEM. Detailed mapping of the fracture surface morphology for Heat 278 aged at 400°C for 10,000 h (parameter P = 4.0) showed that approximately 15-20% of the fracture surface was composed of brittle cleavage and the remainder exhibited a ductile dimple morphology. The cleavage-morphology region revealed river

patterns characteristic of a brittle fracture.[13] In comparison, the extent of cleavage in the fracture surface of the specimen aged at 300°C for 10,000 h (parameter P = 3.14) was minimal.

Similar fracture surface mapping was conducted for specimens of Heats 278 and 280, aged at 300°C for 8 yr (parameter P = 3.99 and 3.70 for Heats 278 and 280, respectively). The fracture surface morphologies of the two specimens are shown in Figs. 7 and 8, respectively. The overall low-magnification morphologies [e.g., Fig. 7(A)] of the fracture surfaces did not indicate any appreciable macroscopic deformation during the room-temperature impact failure. Mapping of the high-magnification fractographs showed that ~15 and 40% of the fracture surfaces of Heats 278 and 280, respectively, were of a brittle-cleavage nature [e.g., Figs. 7(C) and 8(C)]. The rest of the fracture surfaces showed ductile morphologies. The characteristic river patterns could be observed in the cleavage regions.

The fractions of the fracture surfaces of the impact test specimens characterized by the cleavage morphology correspond approximately to the ferrite contents of the material, i.e., ~15 and 40% for Heats 278 and 280, respectively. These observations indicate that the ferrite phase has been embrittled by aging for 10,000 h at 400°C or 70,000 h (8 yr) at 300°C. However, aging for shorter times, e.g., 10,000 h at 300°C, did not embrittle the ferrite phase. The results of the fractographic characterization of the ferrite phase are consistent with the TEM observations which indicated that dislocations in the ferrite phase of the embrittled material were immobilized by Type M and X precipitates. Since the ferrite phase is already embrittled after aging at 300°C for ~8 yr, the toughness of the cast stainless steels after aging for a longer time will be determined by either the austenite phase or interactions between the austenite and ferrite phases of the duplex structure.

References

1. H. D. Solomon and T. M. Devine, "Influence of Microstructure on the Mechanical Properties and Localized Corrosion of a Duplex Stainless Steel," in MiCon 78: Optimization of Processing, Properties, and Service Performance Through Microstructural Control, eds. H. Abrams et al., ASTM STP 672 (1979), p. 430.

2. A. Trautwein and W. Gysel, "Influence of Long Time Aging of CF-8 and CF-8M Cast Steel at Temperatures Between 300 and 500 deg. C on the Impact Toughness and the Structure Properties," Spectrum, Technische Mitteilungen aus dem + GF + Konzern, No. 5 (May 1981); also in Stainless Steel Castings, eds. V. G. Behal and A. S. Melilli, ASTM STP 756 (1982), p. 165.

3. G. Baudry and C. Pichard, "Evolution During Long Holding Times at 300 and 450°C of the Mechanical Properties of Austeno-Ferritic Steel Castings and Welded Joints Used in Pressurized Water Nuclear Reactors," in Troisieme Congres National Sur La Technologie Des Appareils a Bression, Vol. 2, Materiaux, A.F.I.A.P. (1980), p. 673.

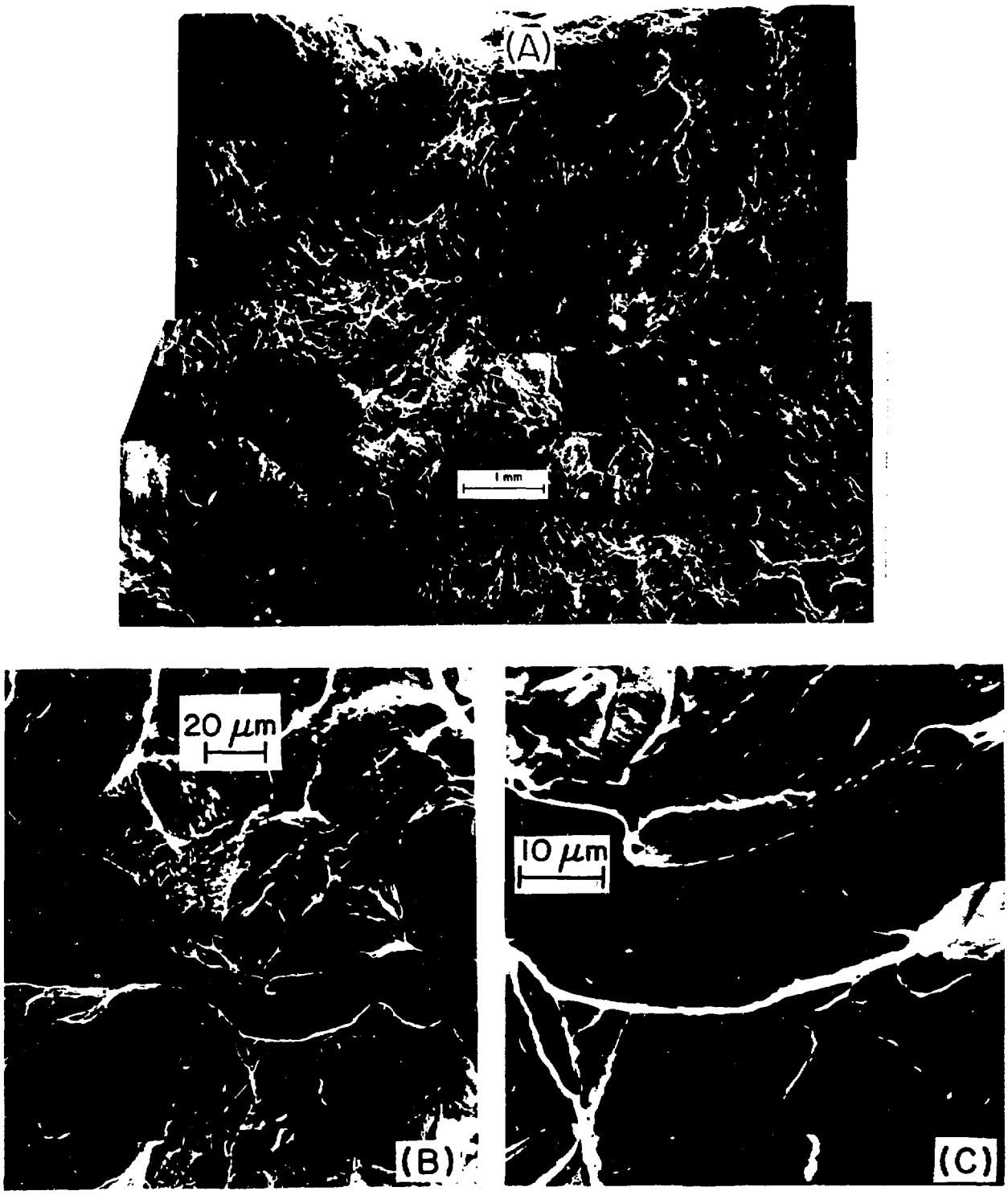

Fig. 7. SEM Fractographs of Cast CF-8 Stainless Steel (Heat 278) after Aging at 300°C for 70,000 h (8 yr) and Impact Failure at 25°C. (A) Overall fracture surface; (B) and (C) higher magnifications of the circled region in (A), showing brittle-cleavage morphology of the ferrite phase.

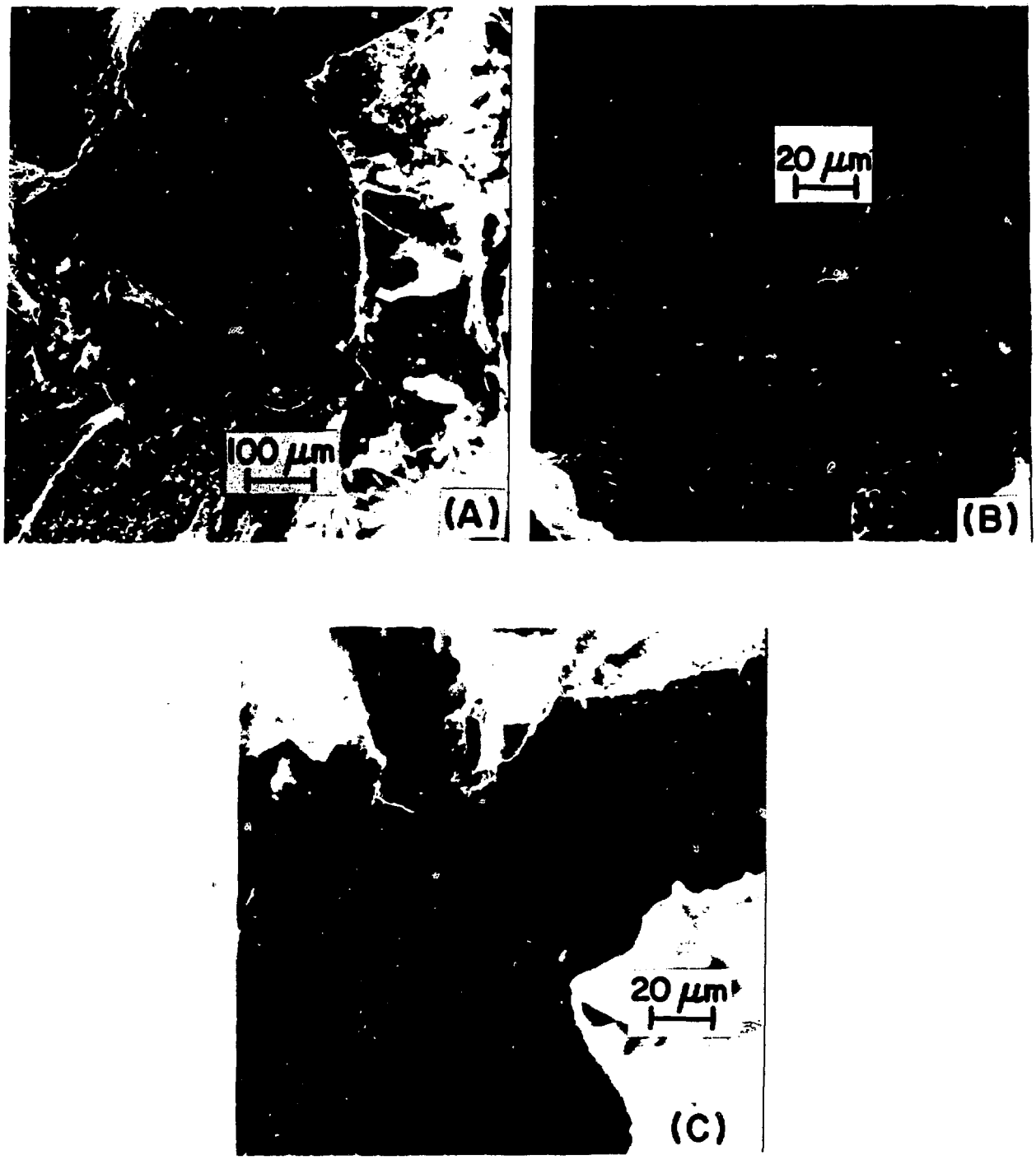

Fig. 8. SEM Fractographs of Cast CF-8 Stainless Steel (Heat 280) after Aging and Impact Failure Similar to Fig. 7. (A) Lower magnification showing both ductile and brittle-cleavage morphologies; (B) and (C) higher magnifications of the cleavage in (A).

4. E. I. Landerman and W. H. Bamford, "Fracture Toughness and Fatigue Characteristics of Centrifugally Cast Type 316 Stainless Steel Pipe after Simulated Thermal Service Conditions," in Ductility and Toughness Considerations in Elevated Temperature Service, ed. G. V. Smith, ASME MPC-8 (1978), p. 99.

5. G. Slama, P. Petrequin, and T. Magep, "Effect of Aging on Mechanical Properties of Austenitic Stainless Steel Castings and Welds," presented at SMIRT Post-Conference Seminar 6, Assuring Structural Integrity of Steel Reactor Pressure Boundary Components, August 29 and 30, 1983, Monterey, CA.

6. P. J. Grobner, "The 885°F (475°C) Embrittlement of Ferritic Stainless Steels," Metall. Trans. 4 (1973), p. 251.

7. T. J. Nichol, A. Dalta, and G. Aggen, "Embrittlement of Ferritic Stainless Steels," Metall. Trans. 11A (1980), p. 573.

8. O. K. Chopra and G. Ayrault, "Aging Degradation of Cast Stainless Steel: Status and Program," in Proc. U. S. Nuclear Regulatory Commission Eleventh Water Reactor Safety Research Information Meeting, NUREG/CP-0048 Vol. 4 (1984), p. 152.

9. A. Hendry, Z. F. Mazur, and K. H. Jack, "Influence of Nitrogen on 475°C Embrittlement of High-Chromium Ferritic Steels," Met. Sci. 13 (1979), p. 482.

10. M. Courtnall and F. B. Pickering, "The Effect of Alloying on 475°C Embrittlement," Met. Sci. 10 (1976), p. 273.

11. Kernkraftwerke Gundremmingen Betriebsgesellschaft, private communication.

12. O. K. Chopra and G. Ayrault, Long-term Embrittlement of Cast Duplex Stainless Steels in LWR Systems: Annual Report, October 1982-September 1983, Argonne National Laboratory, NUREG/CR-3857, ANL-84-44 (1984).

13. O. K. Chopra and H. M. Chung, "Long-Term Embrittlement of Cast Duplex Stainless Steels in LWR Systems," in Light-Water-Reactor Safety Materials Engineering Research Programs: Quarterly Progress Report, January-March 1984, Argonne National Laboratory, NUREG/CR-3998 Vol. I, ANL-84-60 Vol. I (1984), p. 52.